J Physiol 586.22 (2008) pp 5437–5453

The Journal of Physiology

Low expression of Kv7/M channels facilitates intrinsic and network bursting in the developing rat hippocampus

Victoria F. Safiulina[1], Paola Zacchi[1], Maurizio Taglialatela[2,3], Yoel Yaari[4] and Enrico Cherubini[1]

[1] *Neuroscience Programme, International School for Advanced Studies, Trieste, Italy*
[2] *Department of Neuroscience, University of Naples Federico II, Naples, Italy*
[3] *Department of Health Science, University of Molise, Campobasso, Italy*
[4] *Department of Physiology, Hebrew University–Hadassah School of Medicine, Jerusalem, Israel*

Early in development, network activity in the hippocampus is characterized by recurrent synchronous bursts, whose cellular correlates are giant depolarizing potentials (GDPs). The propensity for generating GDPs is attributed to GABAergic synaptic transmission being depolarizing and excitatory in neonatal neurons. However, developmental regulation of intrinsic conductances may also influence GDPs generation. A likely candidate is the non-inactivating, low-threshold, muscarinic-sensitive K^+ current (M current; I_m), which down-regulates intrinsic bursting activity in adult hippocampal pyramidal neurons. Western blot analysis of homogenates of the CA3 hippocampal region showed that expression of the Kv7.2 subunit, one of the constituents of neuronal M channels, is weak in neonatal neurons, and markedly increases after the first postnatal week. Likewise, the density of I_m was very low in neonatal CA3 pyramidal cells and increased later on. Spontaneously occurring intrinsic bursts in neonatal neurons were longer and more robust, and recurred more regularly, than in juvenile neurons. The I_m blocker linopirdine only mildly affected intrinsic bursting in neonatal neurons, but strongly facilitated and regularized it in juvenile neurons. We conclude that the low expression of Kv7/M channels and the depolarizing action of GABA early after birth enhance intrinsic bursting and neuronal synchronization leading to generation of GDPs within the hippocampal network.

(Received 2 May 2008; accepted after revision 17 September 2008; first published online 18 September 2008)
Corresponding author E. Cherubini: Neurobiology Sector, International School of Advanced Studies (SISSA), Ed. Q1 Area Science Park, S.S.14 Km 163.5; 34012 Basovizza (Trieste) Italy. Email: cher@sissa.it

Correlated neuronal activity constitutes a hallmark of developing networks. In the immature hippocampus, the so-called giant depolarizing potentials (GDPs) represent a primordial form of synchrony between neurons, which precedes more organized forms of activity such as theta and gamma rhythms (Buzsaki & Draguhn, 2004). In CA3 pyramidal cells, GDPs are readily observed in the first postnatal week and disappear thereafter (Ben-Ari *et al.* 1989). When recorded from a single neuron, GDPs are characterized by recurrent depolarizing potential shifts with superimposed fast action potentials, separated by silent periods (Ben-Ari *et al.* 1989). During GDPs, intracellular Ca^{2+} concentration rises, as Ca^{2+} enters the cell through voltage-dependent Ca^{2+} channels and *N*-methyl-D-aspartate (NMDA) receptors (Leinekugel *et al.* 1997). GDP-associated Ca^{2+} waves have been proposed to control the number of functional GABAergic and glutamatergic synapses, thus contributing to the structural refinement of the neuronal connectivity and to the establishment of the adult neuronal circuit (Lauri *et al.* 2003; Colin-Le Brun *et al.* 2004; Kasyanov *et al.* 2004; Represa & Ben-Ari, 2005; Mohajerani *et al.* 2007).

The generation of GDPs in the neonatal hippocampus is enabled by the synergistic action of synaptically released glutamate and GABA, both of which are depolarizing and excitatory at this developmental stage (Cherubini *et al.* 1991; Ben-Ari, 2002). Another key factor contributing to GDP generation is the presence of intrinsically bursting neurons, which by virtue of their spontaneous discharge and large spike output can drive other neurons to fire in synchrony (Menendez de la Prida & Sanchez-Andres, 2000; Sanabria *et al.* 2001; Sipila *et al.* 2005). It has been shown recently (Yue & Yaari, 2004, 2006) that the propensity for intrinsic bursting in hippocampal pyramidal neurons is tightly regulated by the density of the muscarinic-sensitive, low voltage-activated, non-inactivating K^+ current (M-current or I_m; Brown & Adams, 1980; Halliwell & Adams, 1982). This current is underlain by homomeric or heteromeric tetramerization of subunits encoded by the Kv7 gene family (Wang

DOI: 10.1113/jphysiol.2008.156257

et al. 1998; Shapiro *et al.* 2000; Selyanko *et al.* 2000) and mutations of Kv7.2 or Kv7.3 genes are responsible for benign familial neonatal convulsions (BFNC), a rare autosomal-dominant form of epilepsy of the newborns characterized by onset of seizures around the third day after birth and their disappearance within the third month of life (Charlier *et al.* 1998).

Here we have hypothesized that GDP generation by neuronal networks in the neonatal hippocampus is enabled not only by the excitatory nature of GABAergic transmission, but also by a low density of Kv7/M channels at this developmental stage. According to this hypothesis a deficiency in Kv7/M channels has a disinhibitory action on intrinsically bursting neurons, enhancing their potential of recruiting other neurons into synchronized bursting. We tested this hypothesis in CA3 pyramidal cells using selective Kv7/M channel antibodies and modulators. Our results show that the density of I_m is comparatively low during the first postnatal week, when GDPs are generated, and that the subsequent developmental increase in I_m density contributes to GDP disappearance during the second postnatal week.

Methods

All experiments were carried out in accordance with the European Community Council Directive of 24 November 1986 (86/609EEC) and were approved by the local authority veterinary service.

Western blotting

Animals were decapitated after being anaesthetized with an I.P. injection of urethane (2 g kg^{-1}). The brain was removed from the skull and the hippocampus was dissected free. Hippocampal slices (500 μm tick) were cut with a vibrating microtome. Under a dissecting microscope, the CA3 region was isolated from the rest of the hippocampus and suspended in homogenization buffer (calcium and magnesium-free phosphate buffered saline (PBS), supplemented with complete protease inhibitors (Roche Molecular Biochemicals, Indianapolis, IN, USA) and 1 mM dithiothreitol followed by homogenization with a glass tissue homogenizer. Crude membranes were prepared by differential centrifugation, followed by tissue lysis using 500 μl RIPA buffer (150 mM NaCl, 50 mM Tris-HCl (pH 7.4), 1% Triton X-100, 1% sodium deoxycholate, 0.1% SDS) over 10 min. Solutions were centrifuged for 30 min at 20 000 *g* at 4°C and Western Blot was performed following standard protocol. Supernatants were resolved on 10% SDS-PAGE gel and blotted onto nitrocellulose membranes. Membranes were blocked with 5% milk, 0.1% Tween-20 in TBS for 1 h followed by overnight incubation with polyclonal antibodies against the Kv7.2 channel (Alomone labs, Jerusalem, Israel) at 4°C, followed by incubation with appropriate secondary antibodies. Visualization was performed using chemiluminescence (Amersham, Freiburg, Germany). An anti-β-tubulin III antibody (Sigma, Milan, Italy) was used to check for equal protein loading, following the same procedure.

To quantify Western blot signals, band density was measured using CorelDraw Photo Paint software (Corel, Ottawa, Ontario, Canada) and normalized with respect to controls.

Slice preparation

Experiments were performed on hippocampal slices obtained from neonatal (postnatal day P0–P6) and juvenile (P14–P21) Wistar rats as previously described (Gasparini *et al.* 2000). Briefly, after being anaesthetized with an I.P. injection of urethane (2 g kg^{-1}), the brain was quickly removed from the skull and placed in ice-cold artificial cerebrospinal fluid (ACSF) containing (in mM): NaCl 130, KCl 3.5, NaH_2PO_4 1.2, $NaHCO_3$ 25, $MgCl_2$ 1.3, $CaCl_2$ 2, glucose 25, saturated with 95% O_2 and 5% CO_2 (pH 7.3–7.4). Transverse hippocampal slices (400–500 μm thick) were cut with a vibrating microtome and stored at room temperature (22–24°C) in a holding bath containing the same solution as above. After a recovery period of at least 1 h, an individual slice was transferred to the recording chamber where it was continuously superfused with oxygenated ACSF at a rate of 2–3 ml min^{-1} at 33–34°C.

Electrophysiological recordings

Whole cell patch clamp recordings (in current- and voltage-clamp mode) were obtained from the soma of visually identified CA3 pyramidal neurons. Principal cells were also identified on the basis of their characteristic firing pattern: they accommodated in response to long depolarizing current pulses. We used an Axopatch 1D amplifier (Axon Instruments, Union City, CA, USA), or in some experiments ($n = 16$), a Multiclamp 700A amplifier (Axon Instruments) to avoid distortion of fast signals like action potentials (Magistretti *et al.* 1996). Patch electrodes were pulled from borosilicate glass capillaries (Hingelberg, Malsfeld, Germany). They had a resistance of 5–7 MΩ when filled with an intracellular solution containing (in mM): KCl 140, Hepes 10, EGTA 1, MgATP 2, $MgCl_2$ 2 (pH 7.3 with NaOH). No significant differences in burst duration and number of intraburst spikes were found using the two amplifiers and therefore data were pooled. The term burst refers to a high-frequency (> 100 Hz) cluster of two or more spikes capping a distinct slow depolarizing potential and followed be a lengthy pause in firing (see below, Fig. 6*A* and *B*).

Kv7/M currents were recorded under voltage clamp conditions at 33–34°C using the perforated patch technique (Rae *et al.* 1991) to preserve the intracellular integrity of the neurons. To this end, a stock solution of nystatin (60 mg ml^{-1}) was prepared in dimethyl sulfoxide (DMSO) and diluted in the recording solution immediately before use yielding a final concentration of 125–250 μg ml^{-1}. Capacitance currents were continuously monitored by applying 5–10 mV pulses from a holding potential of −70 mV. To minimize voltage error in voltage-clamp recordings, this was usually compensated by 75–80%. If series resistance changed > 15% during the experiments, the data were discarded (the series resistance value was 4.6 ± 0.4 MΩ). To minimize contamination with other voltage-dependent channels, Kv7/M currents were recorded in the presence of TTX (1 μM), ZD 7288 (20 μM) and $CdCl_2$ (500 μM) to block sodium, I_h, Ca^{2+} and Ca^{2+}-dependent K^+ currents, respectively. In these cases NaH_2PO_4 was omitted from the bathing solution.

The Kv7/M currents were activated either by applying 1 s hyperpolarizing voltage steps from a holding potential of −20 mV to −100 mV every 7 s in 10 mV increments or 1 s depolarizing voltage steps from a holding potential of −80 mV to +30 mV and back to −40 mV, every 7 s in 10 mV increments using pCLAMP 9.2 (Axon Instruments).

Extracellular field potential recordings were performed using conventional glass microelectrodes (tip diameter 5–10 μM) filled with the standard ACSF and placed into CA3 stratum pyramidale.

Chemicals and drugs

Drugs used were: D-(−)-2-amino-5-phosphonopentaoic acid (D-AP5), 6,7-dinitroquinoxaline-2,3-dione (DNQX), 4-(*N*-ethyl-*N*-phenylamino)-1,2-dimethyl-6-(methylamino) pyrimidinium chloride (ZD 7288), picrotoxin, bumetanide, all purchased from Tocris Cookson Ltd (Bristol, UK), tetrodotoxin (TTX, purchased from Latoxan, Valence, France), nystatin and linopirdine (purchased from Sigma, Milan, Italy). *N*-(2-Amino-4-(4-fluorobenzylamino)-phenyl)-carbamic acid ethyl ester (retigabine) was from ASTA Medica (Radebeul, Germany), 10,10-bis(4-pyridinylmethyl)-9(10H)-anthracenone (XE-991) was from DuPont Pharmaceuticals (Wilmington, DE, USA). All drugs were dissolved in artificial cerebrospinal fluid (ACSF), except DNQX, retigabine, linopirdine, XE-991 and bumetanide, whcih were dissolved in dimethylsulphoxide (DMSO; stock concentration: 10 mM; final concentration in the bathing solution: ≤ 0.1%) and picrotoxin that was dissolved in ethanol.

Drugs were applied in the bath via a three-way tap system, by changing the superfusion solution to one differing only in its content of drug(s). The ratio of flow rate to bath volume ensured complete exchange within 2 min.

Data acquisition and analysis

Data acquisition and analysis were performed using Clampfit 9.2 (Axon Instruments) after digitization with an A/D converter (Digidata 1200, Axon Instruments). Data were sampled at 20 kHz and filtered with a cut-off frequency of 1 kHz. Membrane potentials were corrected for a liquid junction potential of −1.9 mV.

The voltage dependence of activation was assessed by plotting current amplitudes normalized to the maximal current obtained at +30 mV *versus* membrane voltages. The voltage dependence of deactivation was assessed by plotting current amplitudes normalized to the maximal current obtained at +10 mV *versus* membrane voltages. Data points were fitted with a single Boltzmann equation:

$$I/I_{MAX} = 1/\{1 + \exp[(V_{1/2} - V_m)/k]\}$$

where $V_{1/2}$ is the voltage for half-maximum activation and deactivation, V_m is the pulse potential and k is the slope factor.

The activation and deactivation time constants of linopirdine-sensitive currents were obtained by subtracting linopirdine-resistant currents evoked by fixed voltage steps from −80 mV to 0 mV and from −20 mV to −90 mV, respectively, from controls. Current traces were fitted with a double exponential function of the following form:

$$y(t) = A_{fast} \exp(-t/t_{fast} + A_{slow} \exp(-t/t_{slow})$$

where A_{fast} and A_{slow} are the fractions of the fast and the slow component, respectively, and τ_{fast} and τ_{slow} are the fast and the slow time constants. Fits were performed with Clampfit 9.2 (Axon Instruments) and Origin software (v. 6.0; OriginLab Corp., Northampton, MA, USA) which uses Levenberg–Marquardt least-squares.

The size of GDPs or intrinsic bursts was measured by integrating the area underneath the membrane depolarization by placing visually a cursor through the baseline. The autocorrelation histograms were calculated for lag times of 20 s, using Clampfit 9.2 (Axon Instruments).

Values are given as means ± S.E.M. Statistical comparisons of means were made by Student's two tailed *t* test. In some experiments, the non-parametric Wilcoxon and ANOVA tests were used; $P < 0.05$ was selected as the criterion for statistical significance.

Results

Developmental increase in Kv7.2 protein expression in CA3

In a first set of experiments, Western blot analyses were performed on homogenates of the CA3 hippocampal region obtained from P0, P7 and P21 rats ($n = 6$ animals for each age group), using selective antibodies against the Kv7.2 subunit. As shown in Fig. 1, expression of the Kv7.2 protein was low at P0 and progressively increased in the subsequent three weeks.

Developmental changes in I_m in CA3 pyramidal cells

Given that Kv7.2 subunits are thought to represent one of the main components of I_m, we next investigated whether the developmental increase in Kv7.2 protein expression is associated with an increase in I_m density and/or in changes in its functional properties. To that end, whole cell perforated patch-clamp recordings (in voltage- and current-clamp mode; see Methods) were performed from CA3 pyramidal cells from neonatal (P0–P6; $n = 117$) and juvenile rats (P17–P21; $n = 49$). A few experiments were also performed at P14–P16 ($n = 6$). Neonatal and juvenile neurons differed markedly in their passive membrane properties, namely, in resting membrane potential (-48.4 ± 2.3 mV *versus* -64.5 ± 2.3 mV, respectively), in input resistance (505 ± 63 MΩ *versus* 166 ± 12 MΩ, respectively) and in membrane capacitance (25 ± 6.8 pF *versus* 113 ± 8 pF, respectively). The more depolarized membrane potential value obtained in immature neurons could be due to the shunting through the contact between the patch pipette and the membrane (Tyzio *et al.* 2003; see Discussion).

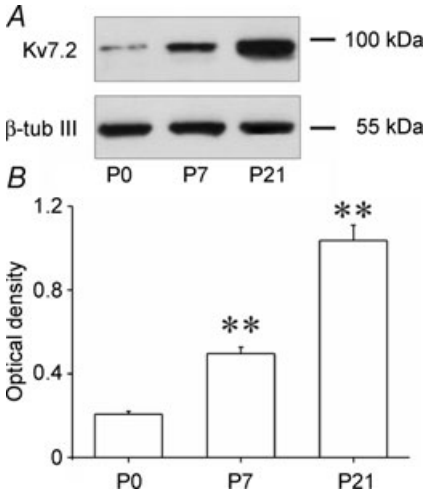

Figure 1. The Kv7.2 subunit is poorly expressed in immature CA3 principal cells
A, example of western immunoblots of homogenates of the hippocampal CA3 region obtained at P0, P7 and P21 probed with polyclonal antibodies against the Kv7.2 subunit. Note the progressive increase of the level of subunit expression with age. Bottom lanes show control loading with β-tubulin III. *B*, bar graph showing Kv7.2 subunit optical density values expressed in arbitrary units at different ages tested normalized with respect to the β-tubulin III signal ($n = 5$; $^{**}P < 0.01$; ANOVA test).

We used two voltage protocols, as well as the selective Kv7/M channel blocker linopirdine (Aiken *et al.* 1995; Lamas *et al.* 1997; Schnee & Brown, 1998), to record I_m in isolation from other voltage-dependent K^+ currents, and to characterize its voltage dependence and kinetics in the two groups of neurons. In both cases the ACSFs contained blockers of Na^+ currents, h current, and Ca^{2+} and Ca^{2+}-dependent K^+ currents (see Methods). The first protocol was an I_m activation protocol. Depolarizing voltage steps (duration 1 s) were applied from a holding potential of -80 mV up to 30 mV in increments of 10 mV. These commands elicited outward currents comprising fast and slowly activating components, the latter attributable to the slowly activating I_m (Halliwell & Adams, 1982). Both components were much larger in juvenile than in neonatal neurons (Fig. 2*A*, Control). Applying 10 μM linopirdine to the ACSF resulted in suppression of the slowly activating outward currents; indeed, K^+ currents in linopirdine-containing ACSF partially inactivated during the depolarizing pulses (Fig. 2*A*, Linopirdine). Subtraction of the latter traces from the control responses yielded the linopirdine-sensitive currents attributable to I_m (Fig. 2*A*, Difference). Because pyramidal cell size increases during the first postnatal weeks (Tyzio *et al.* 2003), we compared the two groups of neurons with respect to I_m density, obtained by normalizing linopirdine-sensitive currents to the cell capacitance (see Methods). As summarized in Fig. 2*B*, linopirdine-sensitive current densities evoked by stepping voltage to -10 mV were substantially and significantly ($P < 0.001$; Wilcoxon's test) greater in juvenile (2.8 ± 0.3 pA pF^{-1}; $n = 7$) than in neonatal neurons (0.6 ± 0.1 pA pF^{-1}; $n = 8$).

To compare the two groups of neurons with respect to the voltage dependence of I_m activation, we plotted linopirdine-sensitive currents (normalized to the maximal current obtained at $+30$ mV) *versus* voltage (I_m–V relations) and fitted them with the Boltzmann equation (Fig. 2*C*; see Methods). The obtained I_m–V relations were significantly different ($P < 0.05$, Wilcoxon's test), disclosing a negative shift of the I_m–V relation during development. We obtained $V_{1/2}$ values of -22.2 ± 2.9 mV and -37.2 ± 7.2 mV for neonatal ($n = 8$) and juvenile neurons ($n = 7$), respectively. The corresponding slope factors (k) were 15.4 ± 1.8 and 21.4 ± 8.6. However, caution should be taken in interpreting the I_m–V relationship particularly in neonates where possible sources of errors can be introduced by the perforated patch-clamp technique (see Discussion on this point).

The second protocol for I_m isolation was an I_m deactivation protocol (Brown & Adams, 1980; Adams & Brown, 1982). The neurons were held at a relatively depolarized potential (−20 mV) to activate Kv7/M channels and to inactivate other classes of voltage-gated K^+ channels. Hyperpolarizing voltage steps (duration 1 s) incrementing by −10 mV down to −100 mV induced slow current 'relaxations' following the instantaneous inward current drops (Fig. 3*A*, Control). In each response the current component undergoing 'relaxation' represents the slow deactivation of I_m. The reversal potentials of the I_M values isolated with this protocol were quite the same in the two groups (-92.5 ± 1.7 mV and -87.7 ± 3.6 mV, respectively; $P > 0.05$) and close to the estimated K^+ equilibrium potential in our experimental conditions ($E_K = -96$ mV). Adding 10 μM linopirdine to the ACSF reduced the holding current (at −20 mV) by 27 ± 7 pA ($n = 5$) and 223 ± 53 pA ($n = 5$) in neonatal and juvenile neurons, respectively ($P < 0.001$; Fig. 3*B*; traces under Linopirdine). Again, the I_m obtained by subtracting linopirdine-resistant currents from control currents were much larger in juvenile than in neonatal neurons at all step potentials (Fig. 3*A*, Difference).

Plotting the linopirdine-sensitive currents obtained by the deactivation protocol (normalized to maximal current obtained at +10 mV) *versus* voltage and fitting them with the Boltzmann equation (Fig. 3*B*; see Methods), again yielded two significantly different I_m–V relations ($P < 0.05$, Wilcoxon's test), with the juvenile I_m–V relation more negative than the neonatal I_m–V relation.

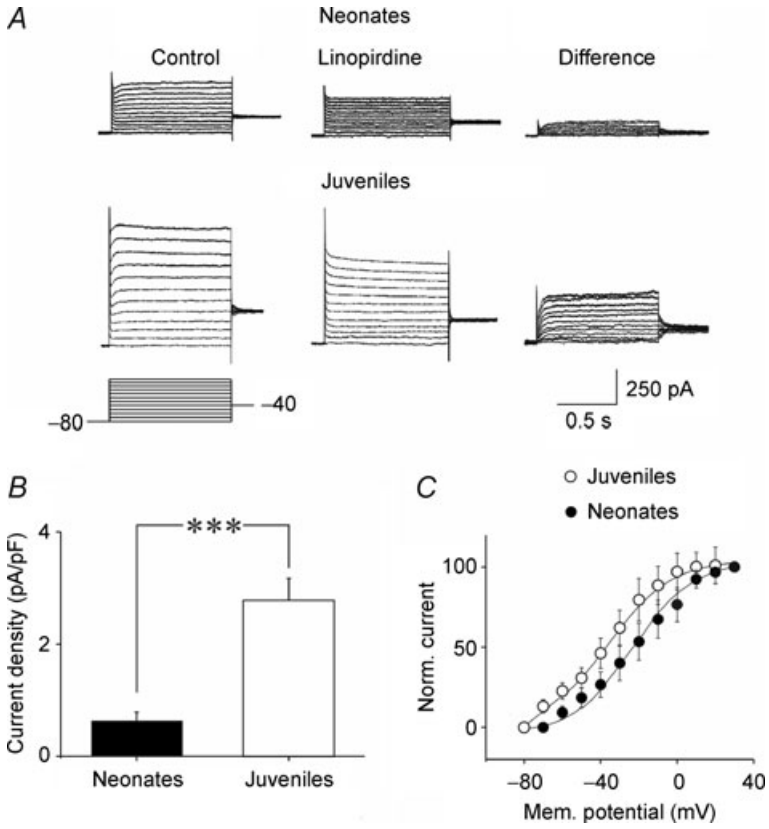

Figure 2. In CA3 pyramidal neurons I_m is developmentally regulated
Examples of current responses recorded from a P1 (upper traces, Neonates) and a P16 (lower traces, Juveniles) CA3 principal cell, by stepping the voltage from −80 mV up to 30 mV in increments of 10 mV, before (Control) and during bath application of 10 μM linopirdine (Linopirdine). The voltage protocol is represented below the current traces. On the right, linopirdine-sensitive currents obtained by subtracting the currents recorded in the presence of linopirdine from control (Difference). *B*, each column represents the density (pA pF^{-1}) of linopirdine-sensitive currents (for voltage steps from −80 mV to −10 mV) normalized to the cell capacitances in neonatal ($n = 8$) and in juveniles neurons ($n = 7$). ***$P < 0.001$. *C*, voltage dependence of linopirdine-sensitive currents (normalized to the maximal currents obtained at +30 mV) obtained in neonatal (filled symbols) and in juvenile neurons (open symbols). Continuous lines, representing the Boltzmann fits of experimental data (each point is the average of 6 individual values), were significantly different ($P < 0.05$; Wilcoxon's test). The voltages at which the currents were half-activated ($V_{1/2}$) were -22.2 ± 2.9 mV and -37.2 ± 7.2 mV for neonatal and juvenile neurons, respectively. The corresponding slope factors were 15.4 ± 1.8 and 21.4 ± 8.6.

The calculated $V_{1/2}$ values were -16.5 ± 3.8 mV and -36.9 ± 5.7 mV for neonatal ($n = 5$) and juvenile neurons ($n = 5$), respectively. The corresponding slope factors (k) were 17.5 ±3.2 and 16.4 ± 6.7. These results are similar to those obtained with the activation protocol.

The fast and slow time constants (τ_{fast} and τ_{slow}) of I_m activation and deactivation were calculated by fitting the linopirdine-sensitive currents obtained from the activation and deactivation protocols with biexponential functions (Fig. 4*A* and *B*). Similar values of τ were found in neonatal ($n = 6$) and juvenile neurons ($n = 6$). Thus, using the activation protocol τ_{fast} and τ_{slow} were 25.1 ± 4.1 ms and 143.1 ± 15.3 ms in neonatal neurons and 37.6 ± 8.5 ms and 147.1 ± 22.3 ms in juvenile neurons (Fig. 4*B*). Likewise, using the deactivation protocol τ_{fast} and τ_{slow} were 20.6 ± 2.6 ms and 119 ± 13.1 ms in neonatal neurons and 23.7 ± 11.4 ms and 152.5 ± 43.1 in juvenile neurons (Fig. 4*C*). The ratio between A_{slow} and A_{fast}, which represent the relative fractions of the respective components (see Methods), were 1.36 ± 0.41 and 0.42 ± 0.16 for the activation protocol ($P > 0.05$; Fig. 4*B*) and 0.89 ± 0.19 and 0.31 ± 0.15 for the deactivation protocol ($P > 0.05$; Fig. 4*C*) in neonatal and juvenile neurons, respectively. The τ_{fast} and τ_{slow} values in neonatal and juvenile neurons were not significantly different ($P > 0.05$ Wilcoxon's test). They were similar to the τ_{fast} and τ_{slow} values of I_m in cultured hippocampal and neuroblastoma cells (Robbins *et al.* 1992; Shahidullah *et al.* 2005).

We next tested the sensitivity of I_m to the Kv7/M channel opener retigabine (Main *et al.* 2000; Rundfeldt & Netzer, 2000; Wickenden *et al.* 2000; Tatulian *et al.* 2001) using the I_m deactivation protocol. As shown in the examples of Fig. 5*A*, retigabine (10 μM) clearly augmented the slowly deactivating components of the outward currents in juvenile neurons, while it had only a minor effect on neonatal neurons (Fig. 5*A*, compare Control and Retigabine). This is particularly evident in the traces obtained by subtracting the currents achieved in the presence of retigabine from the currents in control (Fig. 5*A*, Difference). As summarized in Fig. 5*B*, retigabine-sensitive current densities evoked by stepping voltage from −20 mV to −100 mV were substantially and significantly ($P < 0.05$; Wilcoxon's test) greater in juvenile (2.13 ± 0.3 pA pF^{-1}; $n = 5$) than in neonatal neurons (0.82 ± 0.27 pA pF^{-1}; $n = 5$). In addition, retigabine induced an increase in the holding current (at −80 mV), which was small in neonatal neurons (3.7 ± 1.4 pA; $n = 5$) compared to juvenile neurons (26.2 ± 5.7 pA; $n = 5$; $P < 0.05$; Wilcoxon's test). Plotting the amplitudes of retigabine-sensitive currents (normalized to maximal current obtained at + 10 mV) *versus* voltage and fitting them with the Boltzmann equation again yielded two significantly different I_m–V relations ($P < 0.05$; Wilcoxon's test), with the juvenile I_m–V relation being more negative than the neonatal I_m–V relation (Fig. 5*C*). The calculated $V_{1/2}$ values were -16.6 ± 6.0 mV and -39.8 ± 3.4 mV for neonatal ($n = 5$) and juvenile neurons

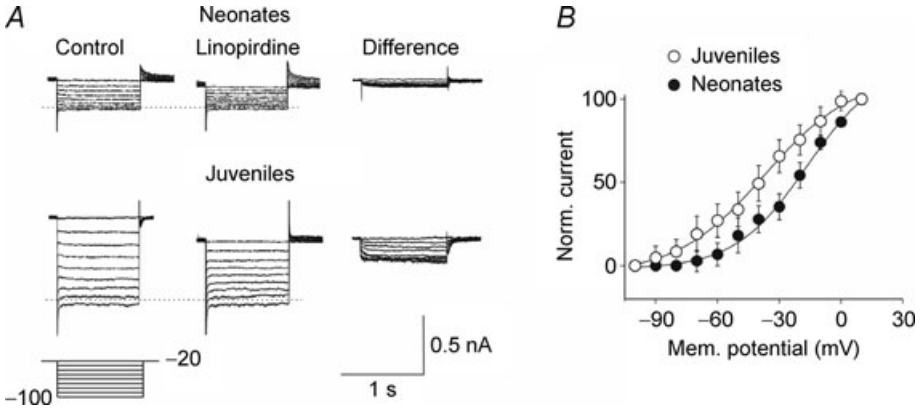

Figure 3. I_m measured with a deactivation protocol
A, examples of deactivation currents recorded from a P1 (upper traces, Neonates) and from a P16 (lower traces, Juveniles) CA3 principal cell. The deactivation protocol (represented below the current traces) consisted in stepping the voltage from −20 mV down to −100 mV in increments of 10 mV, before (Control) and during bath application of 10 μM linopirdine (Linopirdine). On the right, linopirdine-sensitive currents obtained by subtracting the currents recorded in the presence of linopirdine from control (Difference). The horizontal dotted lines mark the I_m reversal potential. *B*, voltage dependence of deactivated linopirdine-sensitive currents (normalized to the maximal currents obtained at +10 mV) obtained in neonatal (filled symbols) and in juvenile neurons (open symbols). Continuous lines, representing the Boltzmann fits of experimental data (each point is the average of 5 individual values) were significantly different ($P < 0.05$; Wilcoxon's test). $V_{1/2}$ values were -16.5 ± 3.8 mV and -36.9 ± 5.7 mV for neonatal and juvenile neurons, respectively. The corresponding slope factors were 17.5 ± 3.2 and 16.4 ± 6.7.

($n = 5$), respectively. The corresponding slope factors (k) were 16.5 ± 4.4 and 24.6 ± 3.2.

Altogether, these results indicate that the expression of Kv7/M channels is low during the first week of postnatal life, and markedly increases within the subsequent weeks.

Intrinsic bursting activity in neonatal *versus* juvenile neurons

Neonatal CA3 pyramidal cells display an intrinsically bursting pattern of firing that plays an instructive pacemaker role in the generation of GDPs (Sipila *et al.* 2005). We compared neonatal and juvenile neurons with respect to this firing mode using patch-clamp recordings in current-clamp mode. Representative recordings from a neonatal (P5) neuron are shown in Fig. 6*A*. The neuron manifested recurrent burst discharges identified as GDPs because their recurrence frequency was independent of the membrane potential (Ben-Ari *et al.* 1989). Thus, at both −90 and −70 mV the recurrence frequencies of these events were the same (0.10 ± 0.004 Hz and 0.10 ± 0.005 Hz, respectively; Fig. 6*A*, top trace). To identify the intrinsic discharge pattern of this neuron, the network-driven discharges were blocked by adding ionotropic glutamate (20 μM DNQX and 50 μM APV) and GABA receptor (100 μM picrotoxin) blockers to the ASCF (Sanabria *et al.* 2001). This revealed recurrent bursting that was blocked by hyperpolarizing the neuron (Fig. 6*A*, bottom trace). In the presence of these blockers, 31 of 71 neonatal neurons (45%) displayed intrinsic bursting activity. At about resting potential, intrinsic bursts recurred at a frequency of 0.33 ± 0.04 Hz ($n = 26$). The proportion of bursting neonatal neurons and the frequency of bursts are similar to those previously described using the cell-attached configuration (Sipila *et al.* 2005). For 10 neurons, the average potential at

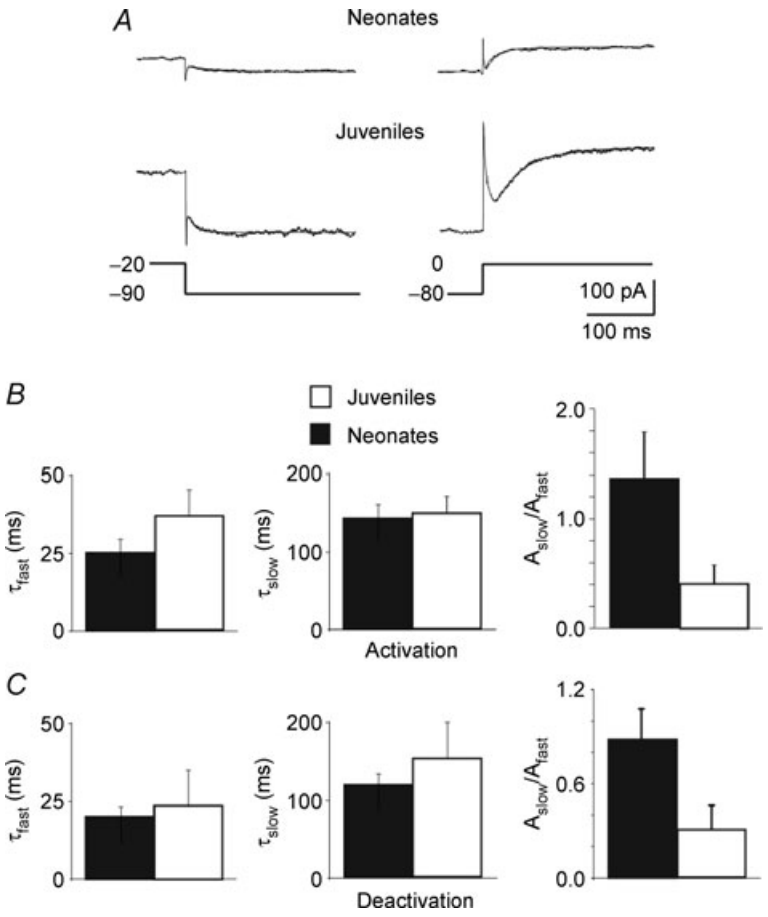

Figure 4. Similar kinetic properties of linopirdine-sensitive currents recorded in neonatal and juvenile neurons
A, linopirdine-sensitive currents deactivated by 1 s voltage step from −20 to −90 mV (left) and activated (right) by 1 s voltage step from −80 to 0 mV. Each trace (average of 3 traces) could be fitted with the sum of a fast and a slow exponential. *B* and *C*, each bar represents the mean fast (τ_{fast}) and slow (τ_{slow}) components as well as their relative fractions A_{slow}/A_{fast} of deactivated (*C*) and activated (*B*) linopirdine-sensitive currents obtained in neonatal (black; $n = 7$) and in juvenile neurons (white; $n = 5$) as in *A*.

which these bursts erupted (i.e. burst 'threshold') was -56 ± 2 mV. Each intrinsic burst was preceded by a slow depolarization, probably underlain by the activation of persistent Na^+ current (Sipila *et al.* 2006*a*) and was followed by a slow afterhyperpolarization (sAHP) that lasted 2.8 ± 0.4 s ($n = 26$). On average, intrinsic bursts lasted 1.4 ± 0.1 s and were associated with 7.3 ± 0.8 spikes per burst. The mean intraburst spike frequency was 5.6 ± 0.6 Hz. A further membrane depolarization increased burst frequency and reduced the amplitude and duration of the sAHPs. The coefficient of variation (CV) of burst intervals was higher than 0.25 for burst frequency lower than 0.20 Hz, and decreased to a stable level when bursts frequency increased to 0.40 Hz (Fig. 6*D*).

The incidence of intrinsic bursters amongst juvenile neurons (23 of 35 neurons; 65%) was higher than in neonatal neurons (Fig. 6*B* and *C*). Although the threshold (-55 ± 3 mV) and the frequency (0.24 ± 0.02 Hz) of intrinsic bursts were not significantly different ($P > 0.5$; Wilcoxon's test) from those of neonatal neurons, burst duration was much shorter (0.49 ± 0.05 s; $P < 0.05$; Fig. 6*E*). In addition, the number of intraburst spikes was much smaller (3.9 ± 0.5; $P < 0.05$; Fig. 6*F*), though their frequency was higher (9.8 ± 2.0 Hz; $P < 0.05$) than in neonatal neurons. As in the latter neurons, the recurrence frequency of intrinsic bursts in juvenile neurons also was not related to the CV of burst intervals (Fig. 6*D*).

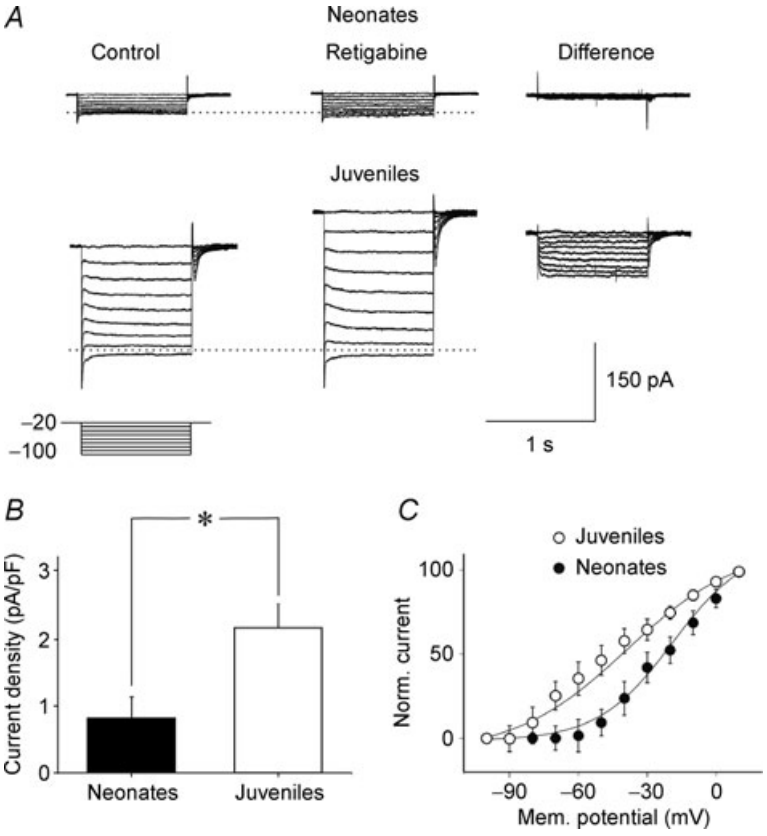

Figure 5. The Kv7/M channel enhancer retigabine potentiates I_m more in juvenile than in neonatal neurons

Examples of deactivating currents recorded from a P1 (upper traces, Neonates) and from a P18 (lower traces, Juveniles) CA3 principal cell. The deactivation protocol (represented below the current traces) consisted in stepping the voltage from -20 mV down to -100 mV in increments of 10 mV, before (Control) and during bath application of 10 μM retigabine (Retigabine). On the right, retigabine-sensitive currents obtained by subtracting the currents recorded in the presence of retigabine from control (Difference). The horizontal dotted lines mark the I_m reversal potential. *B*, each column represents the density (pA pF^{-1}) of retigabine-sensitive currents (for voltage steps from -20 to -100 mV) normalized to the cell capacitances in neonatal ($n = 5$) and in juvenile neurons ($n = 5$). $^*P < 0.05$. *C*, voltage dependence of deactivated retigabine-sensitive currents (normalized to the maximal currents obtained at $+10$ mV) obtained in neonatal (filled symbols) and juvenile neurons (open symbols). Continuous lines represent the Boltzmann fits of experimental data (each point is the average of 4–5 individual values). The $V_{1/2}$ values were -16.6 ± 6.0 mV and -39.8 ± 4 mV for neonatal and juvenile neurons, respectively. These values were significantly different ($P < 0.05$). The corresponding slope factors were 21.4 ± 6.4 and 24.5 ± 3.2.

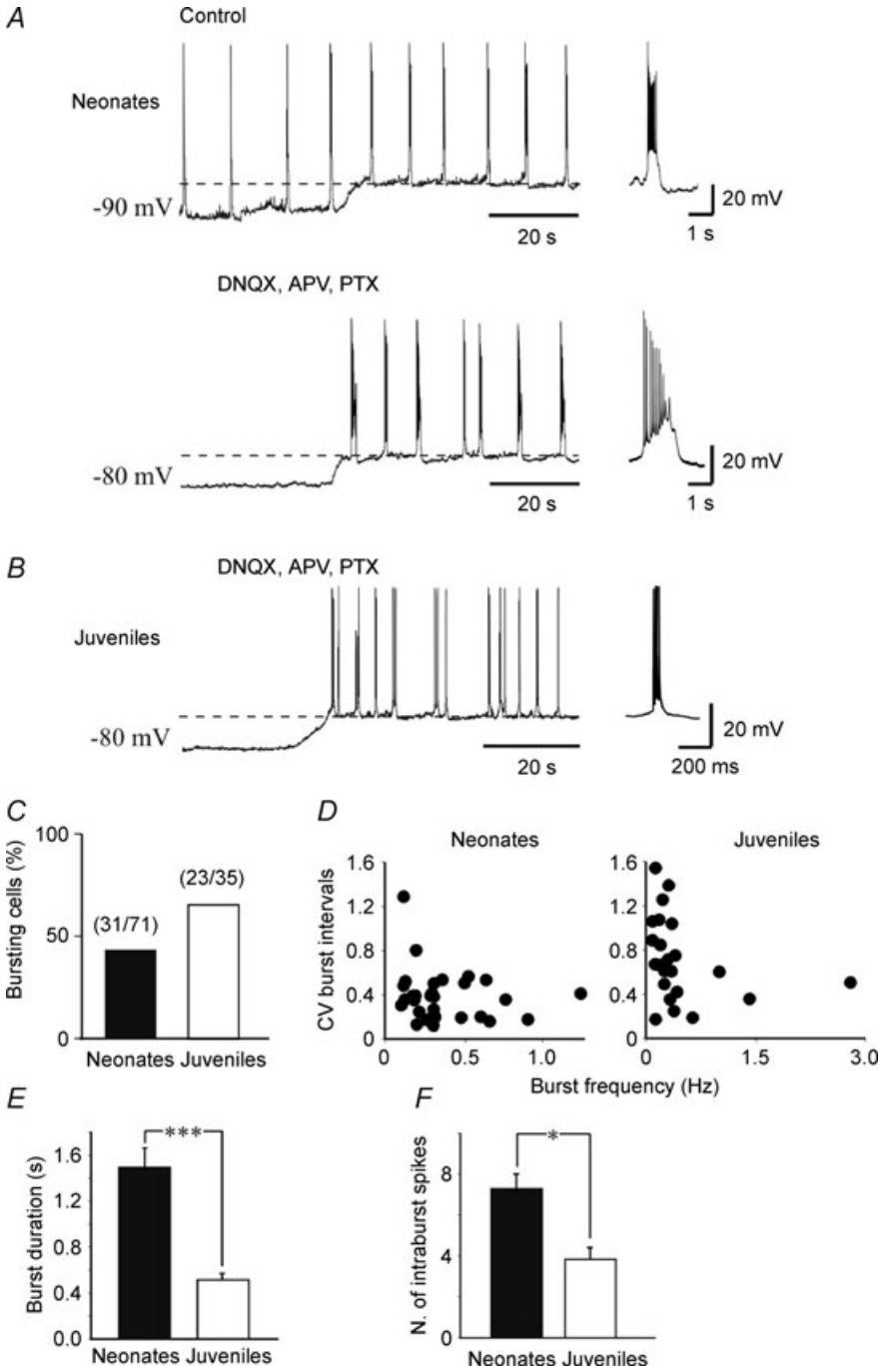

Figure 6. Intrinsic bursting activity in neonatal and juvenile neurons
A, upper trace, GDPs recorded from a CA3 pyramidal cell at P5. The frequency of GDPs did not change by depolarizing the membrane from −90 mV to −70 mV (dashed line) indicating that GDPs are network-driven events. Lower trace, same cell, after blocking synaptic activity and GDPs with DNQX (20 μM), APV (50 μM) and picrotoxin (100 μM). Depolarizing the membrane from −80 mV to −56 mV (dashed line) induced the appearance of intrinsic voltage-dependent bursts, different in shape from GDPs (see individual samples on the right). *B*, representative tracing from a P21 neuron. At this postnatal age, GDPs are not present any more. Depolarizing the membrane to −65 mV (dashed line) in the presence of DNQX, APV and picrotoxin revealed intrinsic bursts which differed in frequency and shape from those recorded in neonatal neurons (see individual burst on the right). *C*, incidence of intrinsic bursts in neonatal and in juvenile neurons. *D*, the coefficient of variation (CV) of interburst intervals plotted against burst frequency in neonatal (left) and in juvenile neurons (right). *E* and *F*, mean burst duration and number of intraburst spikes in neonatal ($n = 26$) and in juvenile neurons ($n = 20$). Note that in juvenile neurons burst duration was significantly shorter and the number of intraburst spikes was significantly smaller than in neonatal neurons. $^{*}P < 0.05$; $^{***}P < 0.001$.

Effects of Kv7/M channel modulators on intrinsic bursting

We next studied the involvement of Kv7/M channels in intrinsic bursting (9 neonatal and 10 juvenile neurons) by monitoring the effects of linopirdine and retigabine on this activity. In these experiments all ACSFs contained ionotropic glutamate and GABA receptor blockers to suppress the synaptically driven GDPs occurring in juvenile neurons. Adding 10 μM linopirdine to the ACSF had more pronounced effects on juvenile than on neonatal neurons. Thus, linopirdine caused a depolarizing shift of 3.4 ± 1.7 mV in neonatal and 5.3 ± 1.5 mV in juvenile neurons. Concurrently, membrane input resistance increased by 13% (from 478 ± 73 MΩ to 542 ± 75 MΩ) in neonatal and by 27% (from 135 ± 14 MΩ to 171 ± 11 MΩ) in juvenile neurons. Likewise, linopirdine induced a 29% increase in the frequency of bursts (from 0.31 ± 0.07 Hz to 0.40 ± 0.11 Hz; $P < 0.05$, paired t test; $n = 9$) in neonatal neurons (Fig. 7*A*) compared to a 109% increase (from 0.20 ± 0.02 Hz to 0.42 ± 0.05 Hz; $P < 0.001$, paired t test; $n = 10$) in juvenile neurons (Fig. 7*B*). It also caused a 30% increase in burst duration (from 1.34 ± 0.08 s to 1.73 ± 0.13 s; $P < 0.05$, paired t test; $n = 9$) in neonatal neurons (Fig. 7*A*) *versus* a 66% increase (0.58 ± 0.13 s to 0.98 ± 0.17 s; $P < 0.05$, paired t test; $n = 10$) in juvenile neurons (Fig. 7*B*). These results indicate that Kv7/M channel activation normally restricts the perpetuation of intrinsic bursts (Yue & Yaari, 2004). This restrictive action is more pronounced in juvenile neurons than in neonatal neurons, consistent with the greater functionality of these channels in the former group.

We also examined how blocking Kv7/M channels affects the regularity of intrinsic bursting in both groups of neurons. To that end we compared autocorrelation plots of burst timing in the absence and in the presence of linopirdine. Figure 7 shows typical examples of intrinsic bursting in neonatal and juvenile neurons. In neonatal neurons, bursts recurred with a certain degree of periodicity, as evidenced in the autocorrelation plot; this periodicity was slightly enhanced by linopirdine (Fig. 7*A*). Overall, linopirdine increased the autocorrelation coefficient from 0.21 ± 0.01 to 0.27 ± 0.02 in these neurons ($n = 9$; $P < 0.01$; paired t test; Fig. 7*C*). In juvenile neurons, intrinsic bursting was less regular than in neonatal neurons (autocorrelation coefficient 0.10 ± 0.02), but linopirdine transformed it into a periodic oscillatory activity, increasing the autocorrelation coefficient to 0.25 ± 0.02 ($n = 10$, $P < 0.001$, paired t test; Fig. 7*B*), similar to that found in neonatal neurons. Linopirdine reduced also the CV of burst intervals from 0.39 ± 0.07 to 0.20 ± 0.02 in neonatal neurons ($P < 0.01$, paired t test), and from 0.81 ± 0.11 to 0.23 ± 0.02 in juvenile neurons ($P < 0.001$, paired t test; Fig. 7*D*). Moreover, this drug caused a significant increase in mean burst duration (Fig. 7*E*) without affecting the number of intraburst spikes (Fig. 7*F*).

In both neonatal ($n = 7$) and juvenile neurons ($n = 8$), addition of retigabine (10 μM) to the ACSF caused a progressive reduction in frequency and duration of intrinsic bursts until they disappeared (Fig. 8; in one exceptional P5 neuron, retigabine only decreased the frequency and the duration of bursts without abolishing them). These effects were associated with a membrane hyperpolarization and a reduction in membrane input resistance, which again were more remarkable in juvenile neurons (9.6 ± 3.2 mV and 43%, respectively) than in neonatal neurons (3.0 ± 0.5 mV and 37%, respectively). Depolarizing the membrane with current injection induced the appearance of isolated action potentials but not intrinsic bursts (data not shown). Addition of linopirdine (10 μM) to the retigabine-containing ACSF restored burst activity in both groups of neurons (Fig. 8).

Together, these data show that although intrinsic bursting occurs more frequently in juvenile neurons, this activity is more robust in neonates, as evidenced by burst duration, number of intraburst spikes, and regularity of bursting. Moreover, blocking Kv7/M channels facilitates intrinsic bursting more strongly in juvenile than in neonatal neurons, corresponding to the developmental increase in the functionality of these channels.

Effects of Kv7/M channel modulators on GDPs

All neonatal neurons tested ($n = 23$) exhibited GDPs that comprised a depolarizing shift (lasting 0.87 ± 0.05 s) giving rise to several action potentials and often followed by a hyperpolarizing shift. Adding 10 μM linopirdine to the ACSF significantly increased GDP frequency (from 0.09 ± 0.001 Hz to 0.16 ± 0.002 Hz; $n = 8$; $P < 0.05$; two tailed t test; Fig. 9*A* and *C*). Likewise, GDP size, estimated by the area under the depolarizing shift, increased from 47.4 ± 8.0 mV s to 65.8 ± 10.1 mV s; $n = 8$; ($P < 0.001$; Fig. 9*D*). Another conspicuous effect of linopirdine was to increase the regularity of GDP recurrence (Fig. 9*A* and *B*). This effect was quantified by the autocorrelation function and by the CV of GDP intervals. Thus, linopirdine significantly increased the autocorrelation coefficient from 0.09 ± 0.02 to 0.36 ± 0.04 ($n = 9$; $P < 0.001$; Fig. 9*E*) and reduced the CV value from 0.61 ± 0.12 to 0.19 ± 0.04 ($n = 8$; $P < 0.05$; Fig. 9*F*). Similar effects on GDP frequency, duration and area of the depolarizing shift were observed when XE991 (5 μM), another selective Kv7/M channel blocker (Wang *et al.* 1998; Yue & Yaari, 2004), was applied ($n = 6$; data not shown).

We next tested whether I_m blockade could induce the appearance of GDPs at intermediate stages of development

in which they are not normally observed. Linopirdine (10 μM) was applied to hippocampal slices obtained from P14–P16 old rats. In 4/6 cells, linopirdine was able to induce synchronized correlated activity (Fig. 10). However, in these cases, GDPs occurred at very low frequency (0.024 ± 0.008 Hz). During the third postnatal week, similar linopirdine applications failed to trigger GDPs ($n = 4$).

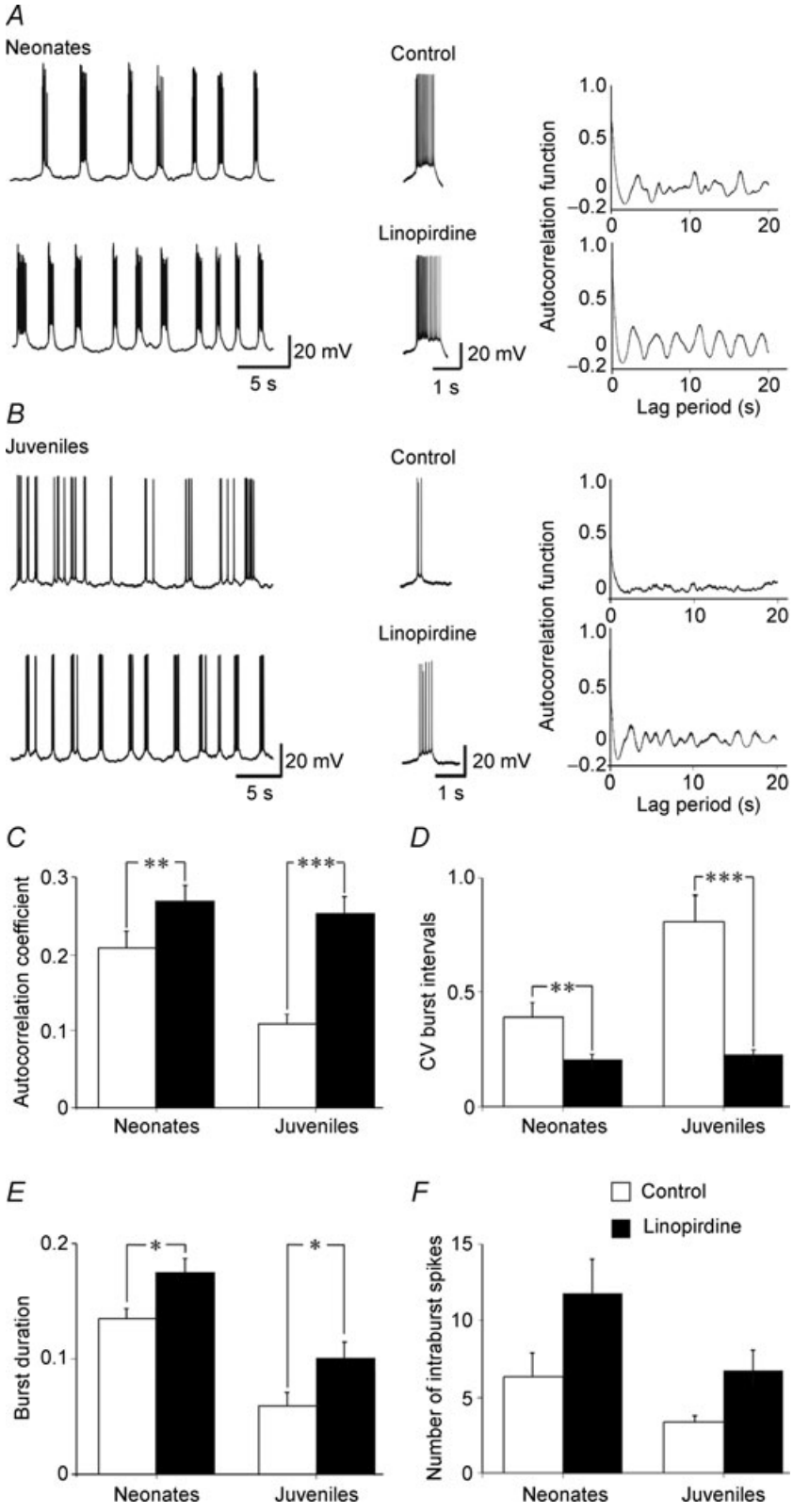

Figure 7. Linopirdine has more pronounced effects on juvenile than in neonatal neurons
A, left, examples of intrinsic bursting activity recorded from a P6 CA3 principal neuron before (upper tracing) and during (lower tracing) bath application of 10 μM linopirdine. Middle, individual bursts in the absence (Control) and in the presence of linopirdine (Linopirdine) shown on an expanded time scale. Right, autocorrelograms for the same cell shown on the left in the absence (upper graph) and in the presence (lower graph) of linopirdine. Linopirdine increased the frequency and the duration of intrinsic bursts which became more regular. *B*, as in *A*, but from a P21 CA3 pyramidal cell. Note differences in burst duration between neonatal and juvenile neurons. In the former neurons, a certain degree of periodicity of bursts activity already existed before the application of linopirdine while this was almost absent in juvenile animals. *C*, summary data showing the autocorrelation coefficients of intrinsic burst activity analysed in neonatal ($n = 9$) and in juvenile neurons ($n = 10$), in the absence (Control) and in the presence of linopirdine (Linopirdine). *D*, CV of bursts intervals measured in neonatal and in juvenile neurons, in the absence and in the presence of linopirdine. *E* and *F*, mean burst duration and number of intraburst spikes before (Control, open bars) and during application of linopiridine (Linopiridine, filled bars) in neonatal ($n = 26$) and in juvenile neurons ($n = 20$). $^{*}P < 0.05$; $^{**}P < 0.01$; $^{***}P < 0.001$.

In neonatal neurons, adding 10 μM retigabine to the ACSF first reduced the frequency and duration of GDPs, then completely suppressed them in all cases ($n = 9$; Fig. 11). GDP suppression was associated with a membrane hyperpolarization of 3.5 ± 0.9 mV, but GDPs could not be restored by depolarizing the membrane 10–20 mV (data not shown). However, GDPs reappeared when linopirdine (10 μM) was added to the retigabine-containing ACSF (Fig. 11).

These data show that although in neonatal neurons I_m is smaller than in juvenile neurons, it still exerts a significant inhibitory action on the generation of GDPs. Blocking this current augments the GDPs in neonatal neurons and can invoke them at an intermediate stage of development in which normally they are no longer generated, though not at a later developmental stage. Conversely, augmentation of this current (with retigabine) suppresses GDPs generation entirely.

Effects of blocking NKCC1 on GDPs

To further evaluate the interplay of GABA action and I_m in modulating GDP activity in neonatal neurons, we tested the consequences of converting GABA action from depolarizing to hyperpolarizing by superfusing the slices for at least 30 min with 10 μM bumetanide, a blocker of the cation–chloride cotransporter NKCC1 (responsible for the accumulation of chloride inside the cell; Dzhala *et al.* 2005; Sipila *et al.* 2006*b*). In agreement with previous studies (Dzhala *et al.* 2005; Sipila *et al.* 2006*b*), bumetanide slightly hyperpolarized the neurons (3–6 mV), shifted GABA reversal potential (E_{GABA}) from -47.6 ± 3.3 mV to -71.5 ± 3.09 mV ($n = 5$; Sivakumaran *et al.* unpublished observations), and blocked GDPs in all slices tested ($n = 7$; Fig. 12). Further application of linopirdine (10 μM) in the presence of bumetanide failed to invoke GDPs. These results show that irrespective of I_m activity, the depolarizing action of GABA is essential for GDPs production during the first postnatal week.

Discussion

In this study we have investigated the developmental regulation of Kv7/M channels responsible for I_m We report that in CA3 pyramidal cells, expression of the Kv7.2 subunit is very low at birth and markedly increases in the subsequent 3 weeks. The low density of I_m in early postnatal life enhances the robustness of intrinsic bursting, which, in conjunction with the depolarizing action of GABA, drives the neuronal network into GDP generation. The developmental increase in I_m density, together with the shift of GABA from the depolarizing to the hyperpolarizing direction, contributes to the disappearance of GDPs in the second postnatal week.

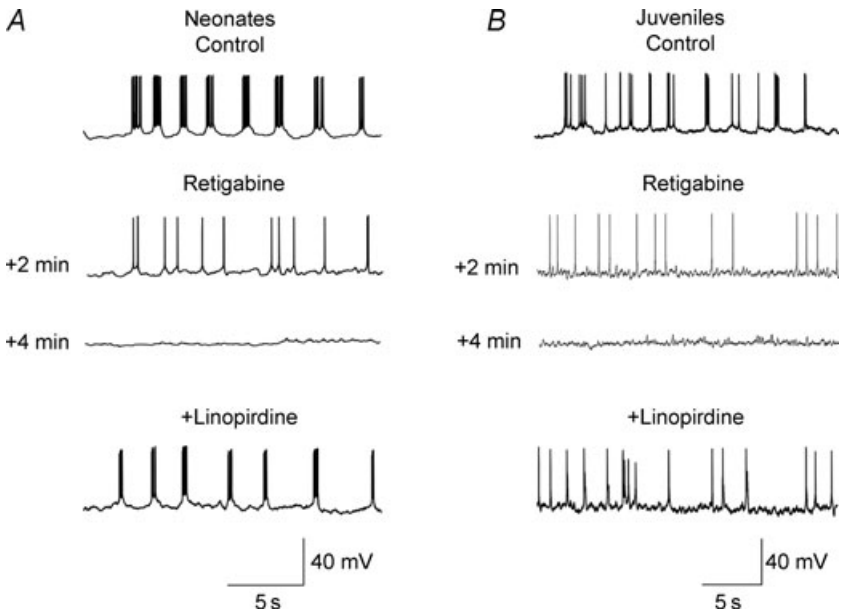

Figure 8. Retigabine completely abolished intrinsic bursts in both neonatal and juvenile neurons
A, intrinsic bursting activity recorded from a CA3 principal cell at P6 before (Control) 2 min and 4 min after bath application of 10 μM retigabine (Retigabine) and after addition of 10 μM linopirdine to retigabine (+Linopirdine). *B*, as in *A* but from a CA3 principal neuron at P17. Note that in both cases, retigabine first reduced the frequency and the duration of intrinsic bursts and then completely abolished them. Intrinsic bursting activity could be restored by adding linopirdine to the bathing solution.

Developmental regulation of Kv7/M channels expression

The postnatal increase in I_m density in CA3 pyramidal cells (Figs 2 and 3) was associated with enhanced Kv7.2 protein expression in hippocampus (Fig. 1), consistent with the notion that this channel subunit is a major determinant of functional neuronal I_m (Wang *et al.* 1998; Shah *et al.* 2002). Previous immunohistochemical studies also disclosed a developmental increase in Kv7.2 and Kv7.3 staining during the first three postnatal weeks (Tinel *et al.* 1998; Geiger *et al.* 2006; Weber *et al.* 2006). This increase was associated with a shift from a widespread staining pattern to a predominantly axonal staining pattern (Weber *et al.* 2006). Indeed, in adult hippocampal pyramidal neurons, Kv7.2 channels are expressed predominantly in the axon initial segment and nodes of Ranvier (Devaux *et al.* 2004; Pan *et al.* 2006). Thus, the developmental regulation of Kv7/M channels involves not only an increase in channel protein, but also targeting of the channels to the axon. Whether other Kv7 subunits, which may also partake in I_m function (Wang *et al.* 1998; Schroeder *et al.* 2000; Shah *et al.* 2002), exhibit a similar developmental profile, is yet unknown.

In addition to manifesting differences in I_m density, the two groups of neurons differed with respect to the voltage dependence of I_m activation, which was about 20 mV more positive in neonatal than in juvenile neurons (Figs 2 and 3). Developmentally regulated differential expression of Kv7.2 splice variants may account for this finding (Smith *et al.* 2001). However, these results should be taken with

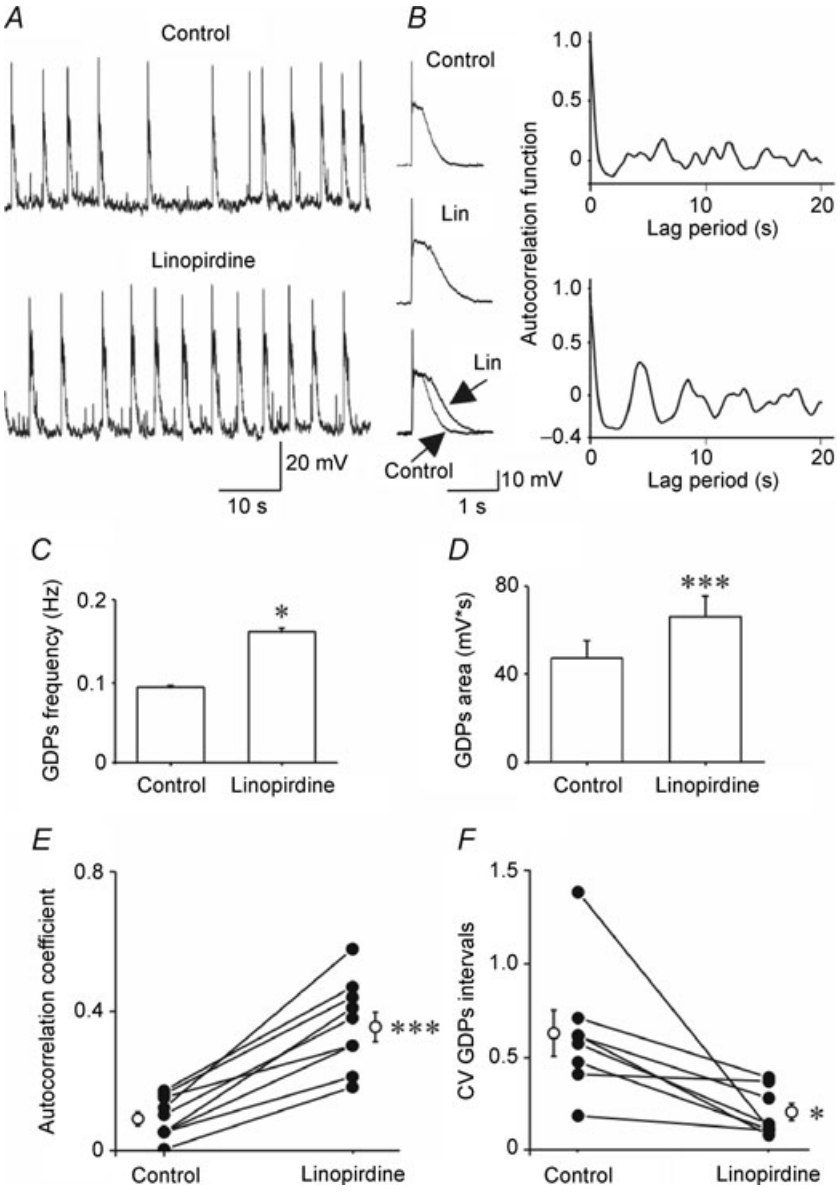

Figure 9. GDPs are modulated by linopirdine
A, GDPs recorded from a CA3 pyramidal cell at P5, before (upper tracing, Control) and during bath application of 10 μM linopirdine (lower tracing, Linopirdine). On the right average of 10 GDPs (represented on an expanded time scale) obtained in the absence (Control) and in the presence of linopirdine (Lin). The two averaged GDPs are superimposed at the bottom. *B*, autocorrelograms for the cell shown in *A*, before (upper graph) and during linopirdine application (lower graph). *C* and *D*, mean GDP frequency (*C*) and area (*D*) in the absence (Control) and in the presence of linopirdine (Linopirdine; $n = 8$ for frequency and area). *E* and *F*, autocorrelation coefficient ($n = 9$, *E*) and CV of GDP intervals ($n = 8$, *F*) for cells recorded between P1 and P6 (filled circles). Open circles represent the mean values. $^*P < 0.05$; $^{***}P < 0.001$.

caution in view of the possible sources of error introduced by the perforated patch-clamp technique. A short-circuit effect of the leak through the contact between the pipette and the membrane may lead to membrane depolarization of several millivolts, particularly in neurons having a high input resistance, such as the small neonatal neurons (see also Tyzio *et al.* 2003; Mohajerani & Cherubini, 2005). In the larger juvenile neurons, the poorer control of voltage may lead to a wrong estimation of membrane potential.

Low density and high threshold of Kv7/M channels potentiates intrinsic bursting in neonatal neurons

We found that intrinsic bursts in neurons manifesting bursting behaviour was much more intense and regular in neonatal than in juvenile neurons. This was evidenced by the longer burst duration (as measured by integrating the depolarizing shift of bursts and by counting the number of intraburst spikes; Fig. 6*E* and *F*), as well as by the lower CV of intervals between bursts (Fig. 7*D*) and the higher spike autocorrelation coefficient (Fig. 7*C*), in neonatal *versus* juvenile neurons. These differences are readily explained by the lower density and the more positive activation voltage of I_m in neonatal *versus* juvenile neurons. In adult neurons, where I_m activates at sub-threshold potentials, it plays a predominant role in

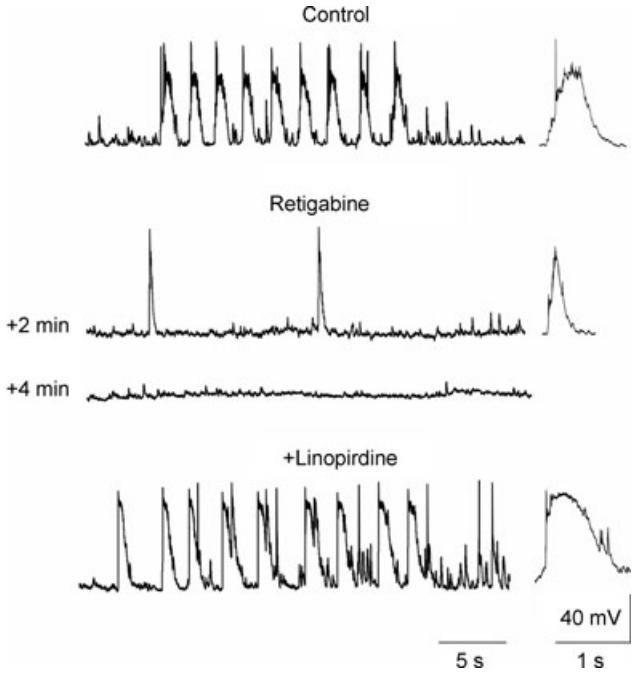

Figure 11. Retigabine completely abolishes GDPs
Representative tracings from a CA3 pyramidal cell at P4 recorded before (Control) and 2 and 4 min after application of 10 μM retigabine (Retigabine) and after addition of 10 μM linopirdine to retigabine (+Linopirdine). Retigabine first reduced and then completely abolished GDPs, which could be restored by adding linopirdine to the extracellular solution.

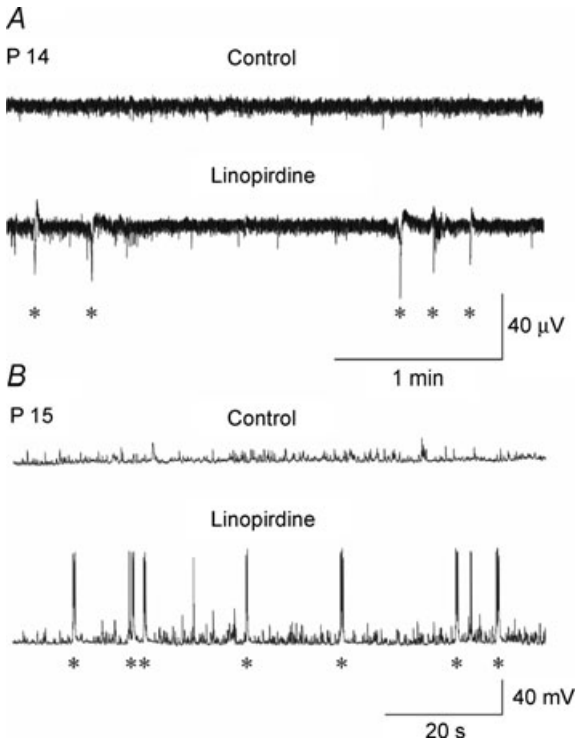

Figure 10. Linopirdine can invoke GDPs at an intermediate developmental stage
Extracellular field potentials (*A*) and whole cell patch clamp recordings (*B*) in hippocampal slices from P14–P15 rats not exhibiting GDPs (Control). Bath application of linopirdine (10 μM for 5 min) induced the appearance of GDPs (asterisks).

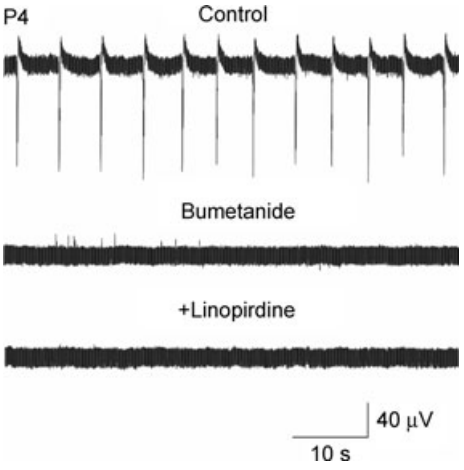

Figure 12. Linopirdine fails to invoke GDPs once these are blocked with bumetanide
Representative extracellular field potential tracings from pyramidal cells (at P4) recorded before (Control), and during bath application of bumetanide (10 μM for 30 min). Note that bumetanide completely blocked GDPs (middle trace). Addition of 10 μM linopirdine to bumetanide (lower trace) failed to invoke the generation of GDPs.

curtailing the spike after depolarization and producing an AHP of medium duration (mAHP; Storm, 1989; Yue & Yaari, 2004; Gu *et al.* 2005). Through these actions I_m would be expected to limit the duration of intrinsic bursts. Our finding that application of linopirdine markedly enhanced and regularized intrinsic bursting activity in juvenile neurons (Fig. 7*B*) suggests that, indeed, I_m plays a major role in burst termination in these neurons. In neonatal neurons, however, linopirdine was much less effective in modulating intrinsic bursting (Fig. 7*C*). This observation is congruent with the reduced availability of Kv7/M channels immediately after birth. The fact that, despite this difference, the fraction of bursters was smaller amongst neonatal than amid juvenile neurons (43% *versus* 66%; Fig. 6*C*) may be due to a developmental increase in the density of low-threshold inward currents, such as persistent Na^+ current and T-type Ca^{2+} current, which provide the depolarizing drive for burst generation (Chen *et al.* 2005; Sipila *et al.* 2005).

Low density and high threshold of Kv7/M channels supports GDP generation in neonatal neurons

Intrinsic bursters, in conjunction with the depolarizing action of GABA, play a critical role in GDP generation in CA3 (Sipila *et al.* 2005). Therefore, it is reasonable to assume that the prolonged intrinsic bursts in neonatal CA3 pyramidal cells, enabled by the low density and high activation voltage of I_m, support GDP generation in these neurons. In addition, the increase in intracellular calcium due to the depolarizing action of GABA (Leinekugel *et al.* 1995) may further increase intrinsic neuronal excitability and GDP generation by inhibiting the Kv7/M channels already present in these neurons (Selyanko & Brown, 1996; Chen & Yaari, 2008). Congruently, blocking I_m with linopirdine or XE991 even further enhanced GDP frequency, duration and regularity (Fig. 9), whereas increasing I_m with retigabine suppressed them entirely (Fig. 11). It should be noted, however, that these effects could result from linopirdine or retigabine acting at Kv7/M channels present not only on pyramidal cells, but also on GABAergic interneurons and/or on presynaptic nerve terminals, where Kv7/M channels have been shown to exert a powerful control on transmitter release (Martire *et al.* 2004; Vervaeke *et al.* 2006; Peretz *et al.* 2007). Apart from that, it is improbable that the developmental enhancement of I_m is the sole reason for the disappearance of GDPs after the first postnatal week. The shift in E_{GABA} towards more hyperpolarized potentials would certainly play a major role in this phenomenon (Ben-Ari *et al.* 1989, 2007; Ben-Ari, 2002), as also demonstrated by the experiments with bumetanide, in which linopirdine was unable to invoke GDPs once GABA's action became hyperpolarizing (Fig. 12). The observation that GDPs could still be invoked by linopirdine in some P14–P16 neurons (Fig. 10) suggests that at this intermediate stage of postnatal development, GABA may still be moderately depolarizing, but I_m has become sufficiently effective in impeding GDP production.

Clinical implications

In humans, loss-of-function mutations in Kv7.2 or Kv7.3 subunits cause the neonatal epileptic disorder benign familial neonatal convulsions (BFNC; Schroeder *et al.* 1998; for reviews see Jentsch, 2000 and Maljevic *et al.* 2008). In neurons harbouring these mutations I_m is reduced, though not abolished (Schroeder *et al.* 1998). An intriguing observation is that in BFNC, seizures begin shortly after birth, and spontaneously disappear within a few months of life. We speculate that the vulnerability of the neonatal brain to these mutations is due not only to the depolarizing action of GABA, but also to the low density and high voltage of activation of neuronal I_m. Likewise, the eventual disappearance of spontaneous seizures in BFNC patients with brain maturation may reflect not only developmental changes in GABA's action, but also changes in Kv7/M channels, similar to those described here.

References

Adams PR & Brown DA (1982). Synaptic inhibition of the M-current: slow excitatory post-synaptic potential mechanism in bullfrog sympathetic neurones. *J Physiol* **332**, 263–272.

Aiken SP, Lampe BJ, Murphy PA & Brown BS (1995). Reduction of spike frequency adaptation and blockade of M-current in rat CA1 pyramidal neurones by linopirdine (DuP 996), a neurotransmitter release enhancer. *Br J Pharmacol* **115**, 1163–1168.

Ben-Ari Y (2002). Excitatory action of GABA during development: the nature of the nurture. *Nat Rev Neurosci* **3**, 728–739.

Ben-Ari Y, Cherubini E, Corradetti R & Gaiarsa JL (1989). Giant synaptic potentials in immature rat CA3 hippocampal neurones. *J Physiol* **416**, 303–325.

Ben-Ari Y, Gaiarsa JL, Tyzio R & Khazipov R (2007). GABA: a pioneer transmitter that excites immature neurons and generates primitive oscillations. *Physiol Rev* **87**, 1215–1284.

Brown DA & Adams PR (1980). Muscarinic suppression of a novel voltage-sensitive K^+ current in a vertebrate neurone. *Nature* **283**, 673–676.

Buzsaki G & Draguhn A (2004). Neuronal oscillations in cortical networks. *Science* **304**, 1926–1929.

Charlier C, Singh NA, Ryan SG, Lewis TB, Reus BE, Leach RJ & Leppert M (1998). A pore mutation in a novel KQT-like potassium channel gene in an idiopathic epilepsy family. *Nat Genet* **18**, 53–55.

Chen S & Yaari Y (2008). Spike Ca^{2+} influx upmodulates the spike afterdepolarization and bursting via intracellular inhibition of K_V7/M channels. *J Physiol* **586**, 1351–1363.

Chen S, Yue C & Yaari Y (2005). A transitional period of Ca^{2+}-dependent spike afterdepolarization and bursting in developing rat CA1 pyramidal cells. *J Physiol* **567**, 79–93.

Cherubini E, Gaiarsa JL & Ben-Ari Y (1991). GABA: an excitatory transmitter in early postnatal life. *Trends Neurosci* **14**, 515–519.

Colin-Le Brun I, Ferrand N, Caillard O, Tosetti P, Ben-Ari Y & Gaïarsa JL (2004). Spontaneous synaptic activity is required for the formation of functional GABAergic synapses in the developing rat hippocampus. *J Physiol* **559**, 129–139.

Devaux JJ, Kleopa KA, Cooper EC & Scherer SS (2004). KCNQ2 is a nodal K^+ channel. *J Neurosci* **24**, 1236–1244.

Dzhala VI, Talos DM, Sdrulla DA, Brumback AC, Mathews GC, Benke TA, Delpire E, Jensen FE & Staley KJ (2005). NKCC1 transporter facilitates seizures in the developing brain. *Nat Med* **11**, 1205–1213.

Gasparini S, Saviane C, Voronin LL & Cherubini E (2000). Silent synapses in the developing hippocampus: lack of functional AMPA receptors or low probability of glutamate release? *Proc Natl Acad Sci U S A* **97**, 9741–9746.

Geiger J, Weber YG, Landwehrmeyer B, Sommer C & Lerche H (2006). Immunohistochemical analysis of KCNQ3 potassium channels in mouse brain. *Neurosci Lett* **400**, 101–104.

Gu N, Vervaeke K, Hu H & Storm JF (2005). Kv7/KCNQ/M and HCN/h, but not KCa2/SK channels, contribute to the somatic medium after-hyperpolarization and excitability control in CA1 hippocampal pyramidal cells. *J Physiol* **566**, 689–715.

Halliwell JV & Adams PR (1982). Voltage-clamp analysis of muscarinic excitation in hippocampal neurons. *Brain Res* **250**, 71–92.

Jentsch TJ (2000). Neuronal KCNQ potassium channels: physiology and role in disease. *Nat Rev Neurosci* **1**, 21–30.

Kasyanov AM, Safiulina VF, Voronin LL & Cherubini E (2004). GABA-mediated giant depolarizing potentials as coincidence detectors for enhancing synaptic efficacy in the developing hippocampus. *Proc Natl Acad Sci U S A* **101**, 3967–3972.

Lamas JA, Selyanko AA & Brown DA (1997). Effects of a cognition-enhancer, linopirdine (DuP 996), on M-type potassium currents (I_{KM}) and some other voltage- and ligand-gated membrane currents in rat sympathetic neurons. *Eur J Neurosci* **9**, 605–616.

Lauri SE, Lamsa K, Pavlov I, Riekki R, Johnson BE, Molnar E, Rauvala H & Taira T (2003). Activity blockade increases the number of functional synapses in the hippocampus of newborn rats. *Mol Cell Neurosci* **22**, 107–117.

Leinekugel X, Medina I, Khalilov I, Ben Ari Y & Khazipov R (1997). Ca^{2+} oscillations mediated by the synergistic excitatory actions of $GABA_A$ and NMDA receptors in the neonatal hippocampus. *Neuron* **18**, 243–255.

Leinekugel X, Tseeb V, Ben-Ari Y & Bregestovski P (1995). Synaptic $GABA_A$ activation induces Ca^{2+} rise in pyramidal cells and interneurons from rat neonatal hippocampal slices. *J Physiol* **487**, 319–329.

Magistretti J, Mantegazza M, Guatteo E & Wanke E (1996). Action potentials recorded with patch-clamp amplifiers: are they genuine? *Trends Neurosci* **19**, 530–534.

Main MJ, Cryan JE, Dupere JR, Cox B, Clare JJ & Burbidge SA (2000). Modulation of KCNQ2/3 potassium channels by the novel anticonvulsant retigabine. *Mol Pharmacol* **58**, 253–262.

Maljevic S, Wuttke TV & Lerche H (2008). Nervous system KV7 disorders: breakdown of a subthreshold brake. *J Physiol* **586**, 1791–1801.

Martire M, Castaldo P, D'Amico M, Preziosi P, Annunziato L & Taglialatela M (2004). M channels containing KCNQ2 subunits modulate norepinephrine, aspartate, and GABA release from hippocampal nerve terminals. *J Neurosci* **24**, 592–597.

Menendez de la Prida L & Sanchez-Andres JV (2000). Heterogeneous populations of cells mediate spontaneous synchronous bursting in the developing hippocampus through a frequency-dependent mechanism. *Neuroscience* **97**, 227–241.

Mohajerani MH & Cherubini E (2005). Spontaneous recurrent network activity in organotypic rat hippocampal slices. *Eur J Neurosci* **22**, 107–118.

Mohajerani MH, Sivakumaran S, Zacchi P, Aguilera P & Cherubini E (2007). Correlated network activity enhances synaptic efficacy *via* BDNF and the ERK pathway at immature CA3–CA1 connections in the hippocampus. *Proc Natl Acad Sci U S A* **104**, 13176–13181.

Pan Z, Kao T, Horvath Z, Lemos J, Sul JY, Cranstoun SD, Bennett V, Scherer SS & Cooper EC (2006). A common ankyrin-G-based mechanism retains KCNQ and Na_V channels at electrically active domains of the axon. *J Neurosci* **26**, 2599–2613.

Peretz A, Sheinin A, Yue C, Degani-Katzav N, Gibor G, Nachman R, Gopin A, Tam E, Shabat D, Yaari Y & Attali B (2007). Pre- and postsynaptic activation of M-channels by a novel opener dampens neuronal firing and transmitter release. *J Neurophysiol* **97**, 283–295.

Rae J, Cooper K, Gates P & Watsky M (1991). Low access resistance perforated patch recordings using amphotericin B. *J Neurosci Methods* **37**, 15–26.

Represa A & Ben-Ari Y (2005). Trophic actions of GABA on neuronal development. *Trends Neurosci* **28**, 278–283.

Robbins J, Trouslard J, Marsh SJ & Brown DA (1992). Kinetic and pharmacological properties of the M-current in rodent neuroblastoma × glioma hybrid cells. *J Physiol* **451**, 159–185.

Rundfeldt C & Netzer R (2000). Investigations into the mechanism of action of the new anticonvulsant retigabine. Interaction with GABAergic and glutamatergic neurotransmission and with voltage gated ion channels. *Arzneimittelforschung* **50**, 1063–1070.

Sanabria ER, Su H & Yaari Y (2001). Initiation of network bursts by Ca^{2+}-dependent intrinsic bursting in the rat pilocarpine model of temporal lobe epilepsy. *J Physiol* **532**, 205–216.

Schnee ME & Brown BS (1998). Selectivity of linopirdine (DuP 996), a neurotransmitter release enhancer, in blocking voltage-dependent and calcium-activated potassium currents in hippocampal neurons. *J Pharmacol Exp Ther* **286**, 709–717.

Schroeder BC, Hechenberger M, Weinreich F, Kubisch C & Jentsch TJ (2000). KCNQ5, a novel potassium channel broadly expressed in brain, mediates M-type currents. *J Biol Chem* **275**, 24089–24095.

Schroeder BC, Kubisch C, Stein V & Jentsch TJ (1998). Moderate loss of function of cyclic-AMP-modulated KCNQ2/KCNQ3 K^+ channels causes epilepsy. *Nature* **396**, 687–690.

Selyanko AA & Brown DA (1996). Intracellular calcium directly inhibits potassium M channels in excised membrane patches from rat sympathetic neurons. *Neuron* **16**, 151–162.

Selyanko AA, Hadley JK, Wood IC, Abogadie FC, Jentsch TJ & Brown DA (2000). Inhibition of KCNQ1–4 potassium channels expressed in mammalian cells via M1 muscarinic acetylcholine receptors. *J Physiol* **522**, 349–355.

Shah MM, Mistry M, Marsh SJ, Brown DA & Delmas P (2002). Molecular correlates of the M-current in cultured rat hippocampal neurons. *J Physiol* **544**, 29–37.

Shahidullah M, Santarelli LC, Wen H & Levitan IB (2005). Expression of a calmodulin-binding KCNQ2 potassium channel fragment modulates neuronal M-current and membrane excitability. *Proc Natl Acad Sci U S A* **102**, 16454–16459.

Shapiro MS, Roche JP, Kaftan EJ, Cruzblanca H, Mackie K & Hille B (2000). Reconstitution of muscarinic modulation of the KCNQ2/KCNQ3 K^+ channels that underlie the neuronal M current. *J Neurosci* **20**, 1710–1721.

Sipila ST, Huttu K, Soltesz I, Voipio J & Kaila K (2005). Depolarizing GABA acts on intrinsically bursting pyramidal neurons to drive giant depolarizing potentials in the immature hippocampus. *J Neurosci* **25**, 5280–5289.

Sipila ST, Huttu K, Voipio J & Kaila K (2006*a*). Intrinsic bursting of immature CA3 pyramidal neurons and consequent giant depolarizing potentials are driven by a persistent Na^+ current and terminated by a slow Ca^{2+} -activated K^+ current. *Eur J Neurosci* **23**, 2330–2338.

Sipila ST, Schuchmann S, Voipio J, Yamada J & Kaila K (2006*b*). The cation–chloride cotransporter NKCC1 promotes sharp waves in the neonatal rat hippocampus. *J Physiol* **573**, 765–773.

Smith JS, Iannotti CA, Dargis P, Christian EP & Aiyar J (2001). Differential expression of KCNQ2 splice variants: implications to M current function during neuronal development. *J Neurosci* **21**, 1096–1103.

Storm JF (1989). An after-hyperpolarization of medium duration in rat hippocampal pyramidal cells. *J Physiol* **409**, 171–190.

Tatulian L, Delmas P, Abogadie FC & Brown DA (2001). Activation of expressed KCNQ potassium currents and native neuronal M-type potassium currents by the anti-convulsant drug retigabine. *J Neurosci* **21**, 5535–5545.

Tinel N, Lauritzen I, Chouabe C, Lazdunski M & Borsotto M (1998). The KCNQ2 potassium channel: splice variants, functional and developmental expression. Brain localization and comparison with KCNQ3. *FEBS Lett* **438**, 171–176.

Tyzio R, Ivanov A, Bernard C, Holmes GL, Ben-Ari Y & Khazipov R (2003). Membrane potential of CA3 hippocampal pyramidal cells during postnatal development. *J Neurophysiol* **90**, 2964–2972.

Vervaeke K, Gu N, Agdestein C, Hu H & Storm JF (2006). Kv7/KCNQ/M-channels in rat glutamatergic hippocampal axons and their role in regulation of excitability and transmitter release. *J Physiol* **576**, 235–256.

Wang HS, Pan Z, Shi W, Brown BS, Wymore RS, Cohen IS, Dixon JE & McKinnon D (1998). KCNQ2 and KCNQ3 potassium channel subunits: molecular correlates of the M-channel. *Science* **282**, 1890–1893.

Weber YG, Geiger J, Kampchen K, Landwehrmeyer B, Sommer C & Lerche H (2006). Immunohistochemical analysis of KCNQ2 potassium channels in adult and developing mouse brain. *Brain Res* **1077**, 1–6.

Wickenden AD, Yu W, Zou A, Jegla T & Wagoner PK (2000). Retigabine, a novel anti-convulsant, enhances activation of KCNQ2/Q3 potassium channels. *Mol Pharmacol* **58**, 591–600.

Yue C & Yaari Y (2004). KCNQ/M channels control spike afterdepolarization and burst generation in hippocampal neurons. *J Neurosci* **24**, 4614–4624.

Yue C & Yaari Y (2006). Axo-somatic and apical dendritic Kv7/M channels differentially regulate the intrinsic excitability of adult rat CA1 pyramidal cells. *J Neurophysiol* **95**, 3480–3495.

Acknowledgements

This work was supported by grants from Ministero Istruzione Universita' e Ricerca (MIUR-PRIN 2005 to E.C.), from the European Union (Project 503221 to EC & E-Rare JTC 2007 and 503038 to M.T.), from Telethon (GGP07125 to M.T.), and from the Deutsche Forschungsgemeinschaft SFB TR3 (Y.Y.). We are grateful to Natasa Dragicevic for participating in some initial experiments.